Available online at www.sciencedirect.com
SCIENCE DIRECT®
ELSEVIER
International Journal of Machine Tools & Manufacture 44 (2004) 1283–1291
INTERNATIONAL JOURNAL OF MACHINE TOOLS & MANUFACTURE DESIGN, RESEARCH AND APPLICATION
www.elsevier.com/locate/ijmactool

Geometric and force errors compensation in a 3-axis CNC milling machine

Chana Raksiri, Manukid Parnichkun *

Asian Institute of Technology, School of Advanced Technologies, P.O. Box 4, Klong Luang, Pathumthani 12120, Thailand

Received 2 February 2004; received in revised form 26 April 2004; accepted 28 April 2004

Abstract

This paper proposes a new off line error compensation model by taking into accounting of geometric and cutting force induced errors in a 3-axis CNC milling machine. Geometric error of a 3-axis milling machine composes of 21 components, which can be measured by laser interferometer within the working volume. Geometric error estimation determined by back-propagation neural network is proposed and used separately in the geometric error compensation model. Likewise, cutting force induced error estimation by back-propagation neural network determined based on a flat end mill behavior observation is proposed and used separately in the cutting force induced error compensation model. Various experiments over a wide range of cutting conditions are carried out to investigate cutting force and machine error relation. Finally, the combination of geometric and cutting force induced errors is modeled by the combined back-propagation neural network. This unique model is used to compensate both geometric and cutting force induced errors simultaneously by a single model. Experimental tests have been carried out in order to validate the performance of geometric and cutting force induced errors compensation model.

Keywords: CNC machine tool accuracy; Geometric error; Cutting force induced error; Machining error; Error compensation

1. Introduction

High accuracy CNC milling machines are required in many manufactures because the demand of precision components and consistency of quality are growing. The most important factor of the precision components is the accuracy of machine tools. Mainly, position errors are originated from geometric, cutting force, dynamic loading, etc. [1,2]. Ramesh et al. [1] analyzed various sources of geometric errors that were usually encountered on machine tools and the methods of error compensation employed in machines.

Many researchers have developed geometric error models. Geometric error is an important source of inaccuracy of CNC milling machine. They measured 21 geometric error components and compensated the systematic errors in CNC milling machines [3–6].

Ehmann et al. [3] presented a method to build a general error model of a multi-axis machine of arbitrary configuration. It is based on the assumption of rigid body motion and utilizes homogenous transformation matrices. Okafor et al. [4] presented derivation of a general volumetric error model, which synthesized both geometric and thermal errors of a vertical milling machine using homogenous transformation matrices of slide axis. They measured 21 geometric error components and compensated the error to validate their error model. Ahn et al. [6] included backlash error to a volumetric error model.

Chen et al. [7] proposed a method to obtain all 21 error components by performing simple displacement measurement along 15 lines using laser interferometer. Chen et al. [8] developed a system which was capable of a diagonal displacement measurement by laser interferometer, when multiple machine axis moved simultaneously, with automatic optic alignment. The results showed that 21 geometric errors of a 3-axis machine could be quickly estimated from the displacement

* Corresponding author. Tel.: +66-2-524-5229; fax: +66-2-524-5697.
E-mail address: manukid@ait.ac.th (M. Parnichkun).

0890-6955/$ - see front matter © 2004 Elsevier Ltd. All rights reserved.
doi:10.1016/j.ijmachtools.2004.04.016

measurements of some determined diagonal lines in the working volume.

The other major cause of inaccuracy in CNC milling machine is error due to cutting force. The error in workpiece is caused either by excessive deformation at the tool and workpiece interface due to cutting action or by deformation of machine tool structure. Ikua et al. [9,10] proposed a theoretical model to predict cutting forces and machining error of convex and concave surfaces in ball-end milling. The machining errors resulted from force induced tool deflections were calculated at various parts of the machined surface. Kim et al. [15] presented a mathematical model to estimate cutting forces and the resultant surface form errors in ball-end milling in various cutting conditions. Cheng et al. [16] studied contour errors of a complete CNC machine system which covered all groups of functions, including trajectory planning, trajectory tracking, cutting process and machine structure dynamics. Yun et al. [11,12] developed a new method that calculated cutting-condition-independent coefficient and its forces over a wide range of cutting conditions and predicted the three-dimensional machined surface errors generated during the peripheral end milling process.

This paper is organized into four sections. The first section discusses the geometric error model of a 3 axis milling machine. The model presented by Ahn et al. [6] is applied. A total of 21 geometric error components are measured by laser interferometer. This model is implemented in an ARD-TB400 CNC milling machine. Geometric error estimation determined by back-propagation neural network is proposed and used in the geometric error compensation model. The geometric error is compensated off-line by modifying the CNC command. Laser interferometer measures the compensated results of two straight lines moving on the x-y plane simultaneously in both forward and backward directions. The second section discusses the cutting force induced error model. It is estimated by back-propagation neural network determined based on a flat end mill behavior observation. The model is used in the cutting force induced error compensation model. A cutting force sensor is developed and applied to measure the cutting forces. The result of machining error due to cutting force is measured by a camera. Various experiments over a wide range of cutting conditions are carried out to verify cutting force and machining error on a 3 axis milling machine. The third section discusses the combination of geometric and cutting force induced errors modeled by the combined back-propagation neural network. It is used to compensate both geometric and cutting force induced errors simultaneously by a single model. Experimental tests are carried out in order to validate the performance of cutting force induced errors compensation.

2. Geometric error model

For the 3-axis milling machine, there are 21 error components. The geometric error model is constructed by using a rigid body model, small angle approximation of the error, and homogeneous transformations. In this paper, the geometric error model of Ahn et al. [6] is applied as follows:

$$\begin{aligned} P_x = {} & \delta_{xx} + \delta_{xy} + \delta_{xz} - \varepsilon_{zx}y + \varepsilon_{yx}z + \varepsilon_{yy}z + S_{xy}y \\ & - S_{xz}z - \delta_{yy}\varepsilon_{zx} - \delta_{yz}\varepsilon_{zx} - \delta_{yz}\varepsilon_{zy} + \delta_{zy}\varepsilon_{yx} \\ & + \delta_{zz}\varepsilon_{yx} + \delta_{zz}\varepsilon_{yy} + \varepsilon_{xy}\varepsilon_{zx}z + \varepsilon_{zx}S_{yz}z + \varepsilon_{zy}S_{yz}z \end{aligned} \quad (1)$$

$$\begin{aligned} P_y = {} & \delta_{yx} + \delta_{yy} - \delta_{zy}\varepsilon_{xx} - \delta_{zz}\varepsilon_{xx} - \delta_{zz}\varepsilon_{xy} + \delta_{xy}\varepsilon_{zx} \\ & - \varepsilon_{zx}S_{xy}y + \delta_{xz}\varepsilon_{zx} - \varepsilon_{zx}S_{xz}z + \delta_{xz}\varepsilon_{zy} \\ & - \varepsilon_{zy}S_{xz}z + \delta_{yz} - S_{yz}z - \varepsilon_{xx}z - \varepsilon_{xy}z + \varepsilon_{yy}\varepsilon_{zx}z \end{aligned} \quad (2)$$

$$\begin{aligned} P_z = {} & \delta_{zx} + \delta_{zy} + \delta_{zz} + \varepsilon_{xx}y + \delta_{yy}\varepsilon_{xx} - \delta_{xy}\varepsilon_{yx} \\ & - \delta_{xz}\varepsilon_{yx} - \delta_{xz}\varepsilon_{yy} + \delta_{yz}\varepsilon_{xx} + \delta_{yz}\varepsilon_{xy} - \varepsilon_{xx}\varepsilon_{xy}z \\ & - \varepsilon_{yx}\varepsilon_{yy}z + \varepsilon_{yx}S_{xy}y - \varepsilon_{xx}S_{yz}z + \varepsilon_{yy}S_{xz}z \\ & - \varepsilon_{xy}s_{yz}z + \varepsilon_{yx}S_{xz}z \end{aligned} \quad (3)$$

where x, y, z are nominal positions, and $\delta_{xx},\delta_{yy},\delta_{zz}$ are their respective positional errors along x, y and z directions, respectively. $\delta_{yx},\delta_{zx},\delta_{xy},\delta_{zy},\delta_{xz},\delta_{yz}$ are straightness errors, where the first subscript refers to error direction and the second refers to moving direction. $\varepsilon_{xx},\varepsilon_{yx},\varepsilon_{zx}$, $\varepsilon_{xy},\varepsilon_{yy},\varepsilon_{zy},\varepsilon_{xz},\varepsilon_{yz},\varepsilon_{zz}$ are angular errors, where the first subscript refer to axis of the rotation error, and the second refers to moving direction. S_{xy},S_{xz},S_{yz} are squareness errors between each pair of axes. Fig. 1

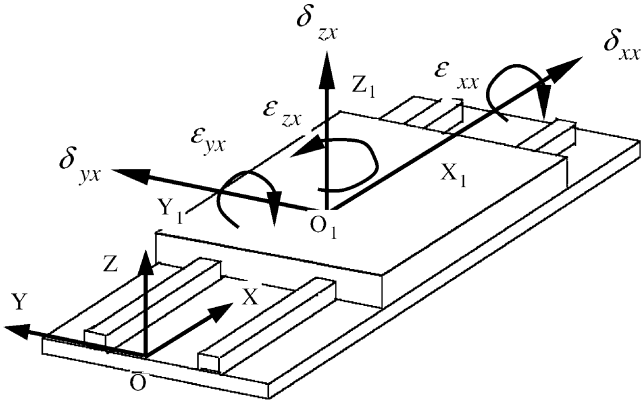

Fig. 1. Schematic of six degrees of freedom error motion of a machine tool system.

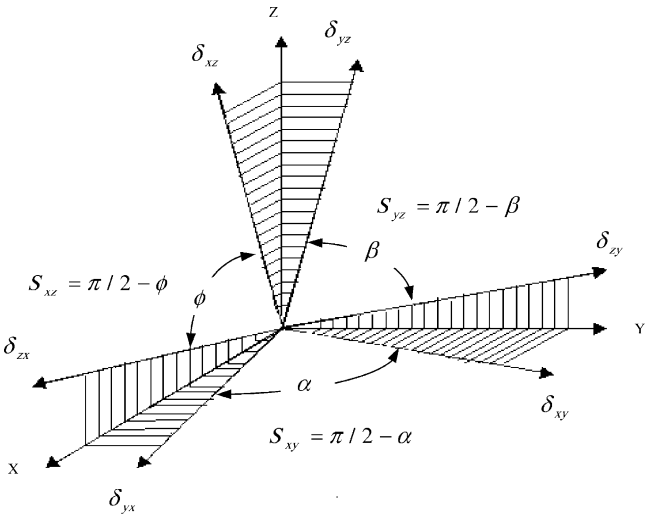

Fig. 2. Squareness errors between each pair of axis.

shows a schematic of six degrees of freedom error motion of a machine system. Fig. 2 shows squareness errors between each pair of axis.

3. Mathematical model of cutting force and machining error

3.1. Cutting force calculation

Yun [13] developed a cutting force model. The three orthogonal force components in the x, y and z axis can be derived from the normal force $(d\vec{F}_n(\phi))$ and the friction force $(d\vec{F}_r(\phi))$ that are proportional to uncut chip thickness as follows:

$$\begin{bmatrix} F_x(i,j,k) \\ F_y(i,j,k) \\ F_z(i,j,k) \end{bmatrix} = B_1 \begin{bmatrix} A_{11} & A_{12} & A_{13} \\ A_{21} & A_{22} & A_{23} \\ A_{31} & A_{32} & A_{33} \end{bmatrix} \times \begin{bmatrix} K_n(i,j,k) \\ K_f(i,j,k)K_n(i,j,k)C_3 \\ K_f(i,j,k)K_n(i,j,k)C_4 \end{bmatrix} \quad (4)$$

where $A_{11} = C_1\cos(\phi - \alpha_r)t_c(i,j,k)$; $A_{12} = \cos(\phi)t_c(i,j,k)$; $A_{13} = -\sin(\phi - \alpha_r)t_c(i,j,k)$; $A_{21} = C_1\sin(\phi - \alpha_r)t_c(i,j,k)$; $A_{22} = \sin(\phi)t_c(i,j,k)$; $A_{23} = \cos(\phi - \alpha_r)t_c(i,j,k)$; $A_{31} = C_2t_c(i,j,k)$ $A_{32} = \cot\theta_h t_c(i,j,k)$; $A_{33} = 0$; $C_1 = \frac{\cos\theta_h}{\sin\theta_{tk}}$; $C_2 = \frac{\sin\theta_h}{\sin\theta_{tk}}$; $C_3 = \sin\theta_h(\sin\theta_C - \cos\theta_C\cot\theta_{tk})$; $C_4 = \frac{\cos\theta_c}{\sin\theta_{tk}}$; $B_1 = \cos\alpha_r\left(\frac{\Delta a}{\cos\theta_h}\right)$; $\cos\theta_{tk} = \sin\alpha_r \cdot \sin\theta_h$; ϕ is the angular position of the cutter; α_r is the rake angle of the cutter; θ_k is the helix angle; K_n,K_f is the specific cutting force; $t_c(i,j,k)$ is the instantaneous uncut chip thickness; θ_c is the chip flow angle; and, Δa is the height of the z-axis disk element.

Cutting force components acting on one flute at an arbitrary cutter rotation angle can be calculated as:

$$\begin{bmatrix} F_x(i,j,k) \\ F_y(i,j,k) \\ F_z(i,j,k) \end{bmatrix} = B_1 \sum_k \begin{bmatrix} A_{11} & A_{12} & A_{13} \\ A_{21} & A_{22} & A_{23} \\ A_{31} & A_{32} & A_{33} \end{bmatrix} \times \begin{bmatrix} K_n(i,j,k) \\ K_f(i,j,k)K_n(i,j,k)C_3 \\ K_f(i,j,k)K_n(i,j,k)C_4 \end{bmatrix} \quad (5)$$

Cutting force components on x, y and z direction at an arbitrary cutter rotation angle can be obtained by summing up the forces acting on each flute at that particular cutter rotation angle:

$$\begin{bmatrix} F_x(i,j,k) \\ F_y(i,j,k) \\ F_z(i,j,k) \end{bmatrix} = B_1 \sum_i \sum_k \begin{bmatrix} A_{11} & A_{12} & A_{13} \\ A_{21} & A_{22} & A_{23} \\ A_{31} & A_{32} & A_{33} \end{bmatrix} \times \begin{bmatrix} K_n(i,j,k) \\ K_f(i,j,k)K_n(i,j,k)C_3 \\ K_f(i,j,k)K_n(i,j,k)C_4 \end{bmatrix} \quad (6)$$

3.2. Cutting deflection calculation

One of the major causes of the machining error is cutting deflection due to cutting force. By assuming the cutter as a cantilever beam, the cutting deflection can be derived as [14]

$$\delta = \frac{F}{6EI}[\langle z_F - z\rangle^3 - \langle L - z\rangle^3 + 3\langle L - z\rangle^2\langle L - z_F\rangle] \quad (7)$$

where F is the cutting force, I is the area moment of inertia of the cutter, E is Young's modulus, L is the overhang, z_F is z-directional position of the applied force, and z is position of the deflection. As shown in Fig. 3, a flat end mill cutter consists of two parts; the flute and the shank parts which can be simplified as a two step cylindrical cantilever beam. The resultant

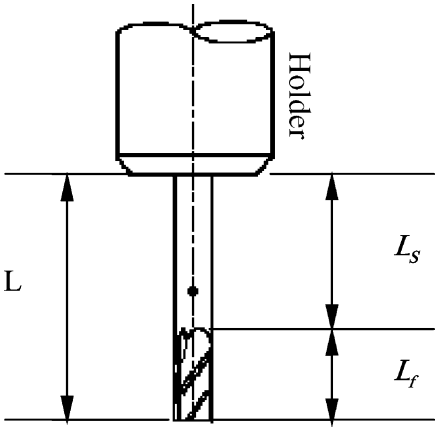

Fig. 3. End mill cutter structure.

cutter bending deflection is

$$\begin{aligned}\delta_t &= \delta_s + \delta_f + \phi_s(L_f - z)\\ &= \frac{F}{6EI}[-(L-L_f)^3 + 3(L-L_f)^2(L-z_F)]\\ &\quad + \frac{F}{6EI_f}[\langle z_F - z\rangle^3 - (L_f - z)^3 + 3(L_f - z)^2(L_f - z_F)]\\ &\quad + \frac{F}{2EI}[-(L-L_f)^2 + 2(L-L_f)(L-z_F)](L_f - z) \quad (8)\end{aligned}$$

where δ_s is deflection of the shank, δ_f is deflection of the flute, ϕ_s is deflection angle of the shank, L_f is length of the flute, and I_f is the moment of inertial of the flute. During flat end mill cuts material in x or y axis, the resultant cutter bending deflection affects the workpiece shape accuracy.

4. Function approximation by back-propagation neural network

Back-propagation neural network is one of the most commonly used neural network structures. It is created by generalizing the Widrow–Hoff [17] learning rule to muti-layer networks and nonlinear differentiable transfer function. It is simple, effective, and found in a wide application such as function approximation. Function approximation applies a network of nodes arranged in two layers, the hidden and output layers. The hidden layer serves to provide means for input relations to be represented in the output. The output layers serve as nodes to buffer output for the model. Two-layer, 1-2-1 network, is shown in Fig. 4. There are two nodes in the hidden layer and one node in the output layer.

Transfer function for the first and second layers can be Log-Sigmoid, Hyperbolic Tangent Sigmoid, Positive Linear, Saturating Linear, or other functions depending on shape of the target. The back-propagation algorithm is a generalization of the LMS (Least Mean Square) algorithm. The algorithm is provided with training set:

$$\{p_1,t_1\},\{p_2,t_2\},\ldots,\{p_Q,t_Q\} \quad (9)$$

where p_q and t_q are the input and target output of the training set. The algorithm modifies the network parameters in order to minimize the mean square error:

$$F(X) = E[e^T e] = E[(t-a)^T(t-a)] \quad (10)$$

where X is the vector of network weights and biases. As with the LMS, the algorithm approximates the mean square error by

$$\hat{F}(X) = (t(k) - a(k))^T(t(k) - a(k)) = e^T(k)e(k) \quad (11)$$

where the expectation of the square error has been replaced by the square error at iteration k. The steepest descent algorithm for the approximated mean square error is

$$\begin{aligned} w^m_{i,j}(k+1) &= w^m_{i,j}(k) - \alpha\frac{\partial\hat{F}}{\partial w^m_{i,j}}\\ b^m_{i,j}(k+1) &= b^m_i(k) - \alpha\frac{\partial\hat{F}}{\partial b^m_i} \quad (12)\end{aligned}$$

where $w^m_{i,j}$, $b^m_{i,j}$ is weight and bias of network, α is the learnig rate. During network training, weights and biases are modified until the approximated mean square error is minimum.

5. Experiments and results

5.1. Geometric error

5.1.1. Geometric error determination

Three positional errors ($\delta_{xx},\delta_{yy},\delta_{zz}$), 6 angular errors ($\varepsilon_{yx},\varepsilon_{zx},\varepsilon_{xy},\varepsilon_{zy},\varepsilon_{xz},\varepsilon_{yz}$), 6 straightness errors ($\delta_{yx},\delta_{zx},\delta_{xy},\delta_{zy},\delta_{xz},\delta_{yz}$) and 3 squareness errors (S_{xy},S_{xz},S_{yz}) were measured by laser interferometer. 3 angular errors ($\varepsilon_{xx},\varepsilon_{yy},\varepsilon_{zz}$) were derived from vertical straightness

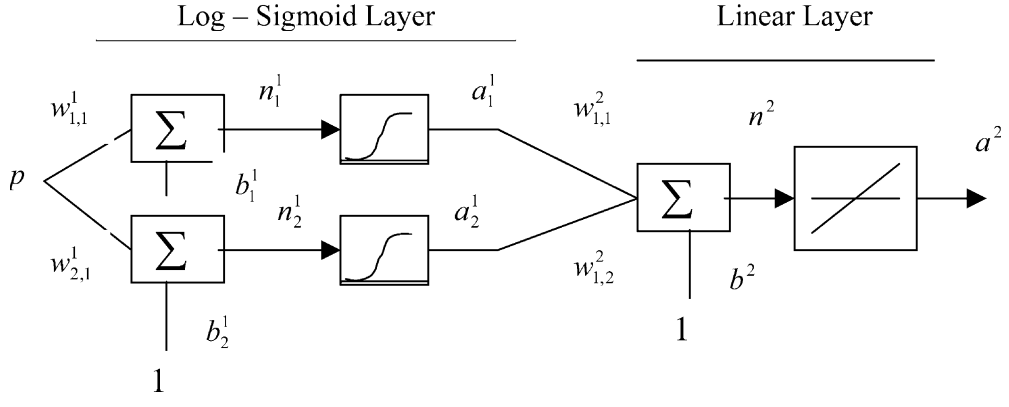

Fig. 4. 1-2-1 Network.

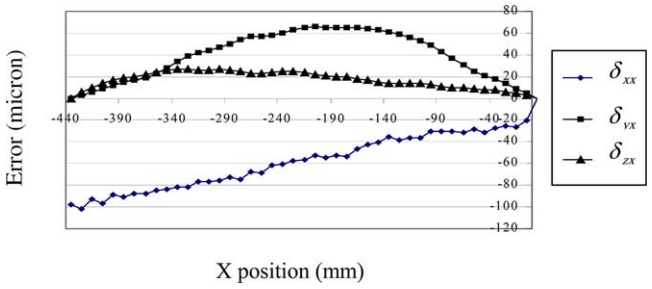

Fig. 5. Position and straightness error along x axis in backward direction.

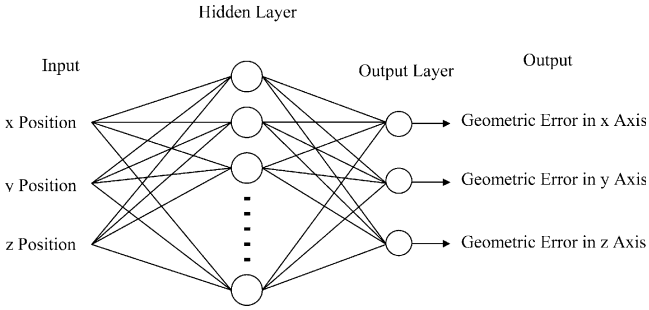

Fig. 7. 3-80-3 Network structure of geometric error model.

errors as referred in the paper of Ahn et al. [6]. All error components in both forward and backward directions were measured. The laser system consisted of the following components: ML10 measurement laser, EC10 environmental compensation unit, interferometer, reflector mirror set, and computer. The error models as functions of positions in x, y and z axis were investigated. Figs. 5 and 6 show some of the error components. Fig. 5 show the position and straightness errors along x axis in backward direction. Fig. 6 show the angular error along y axis in backward direction. Estimation of the error model at an intermediate position between the measured nodes was determined by back-propagation neural network.

5.1.2. Geometric error model

A total of 21 error components were measured directly by laser interferometer in both forward and backward directions. The geometric error of x, y and z axis was calculated by Eqs. (1)–(3) with respect to the measuring position x, y and z. Function approximation by back-propagation neural network was used to approximate geometric error model. The back-propagation neural network structure of geometric error model was shown in Fig. 7. The positions x, y and z of the measuring point were the input of the network and the geometric error in x, y and z axis were the output of the network.

The transfer function of the hidden layer was Hyperbolic Tangent Sigmoid and transfer function of the output layer was Linear. The number of nodes in the hidden layer was varied until the approximated mean square error was satisfied at eighty nodes for both forward and backward directions. After training the network, the geometric error could be determined using this model.

5.1.3. Geometric error compensation

To evaluate the algorithm, the geometric error of two straight lines moving on x-y plane in both forward and backward directions, as illustrated in Fig. 8, was compensated. These lines were represented by parametric equations. The compensation algorithm modified the CNC G-code command by subtracting the expected error from the nominal position to reduce the error.

Laser interferometer was used to measure position errors of the machine following a straight line from point $P_o(x_o,y_o)$ to point $P_1(x_1,y_1)$. Due to position error, the difference between nominal and real distances was identified by laser interferometer. The modified

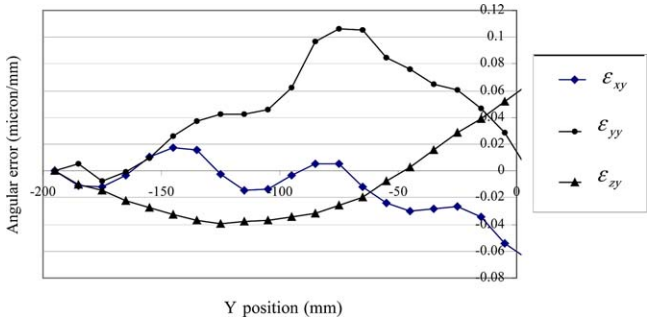

Fig. 6. Angular error along y axis in backward direction.

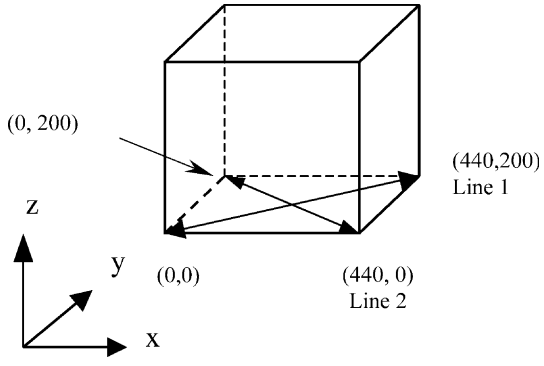

Fig. 8. Line 1 and line 2 in both forward and backward directions.

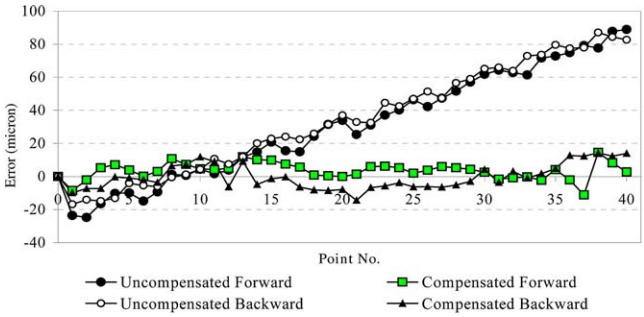

Fig. 9. Position error compensation of line 1 in forward and backward direction.

CNC command could be represented by

$$\text{Position}(x,y)_{\text{modified}} = \text{Position}(x,y)_{\text{nominal}} - \text{Error Position } (x,y) \quad (13)$$

5.1.4. Geometric error compensation results

Fig. 9 shows results of the compensated and uncompensated position error of line 1 in forward and backward directions of the ARD-TB400. The average improvement of line 1 is approximately −34 μm and −28 μm in forward and backward directions, respectively. Fig. 10 shows results of the compensated and uncompensated position error of line 2 in forward and backward directions of the ARD-TB400. The improvement of line 2 is approximately 44 μm and 40 μm in forward and backward directions, respectively.

5.2. Cutting force induced error

5.2.1. Cutting force error determination

In order to investigate the effect of cutting force to machining error, slot and hole in *x*-*y* plane were machined as shown in Fig. 11. Edge A-A was the reference edge. Hole B represented cutting without *x*-*y* plane cutting force effect and slot C represented cutting with *x*-*y* plane cutting force effect. The different distance between edge A-A to end points of hole B and slot C was the machining error due to cutting force.

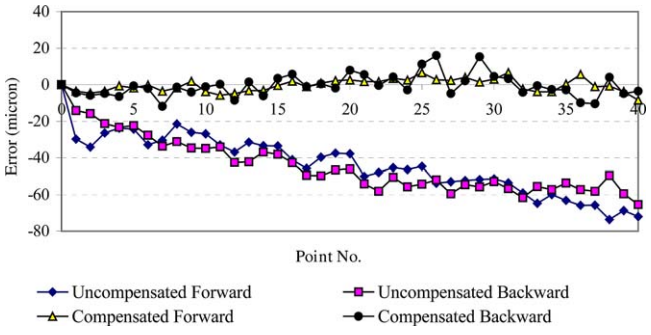

Fig. 10. Position error compensation of line 2 in forward and backward direction.

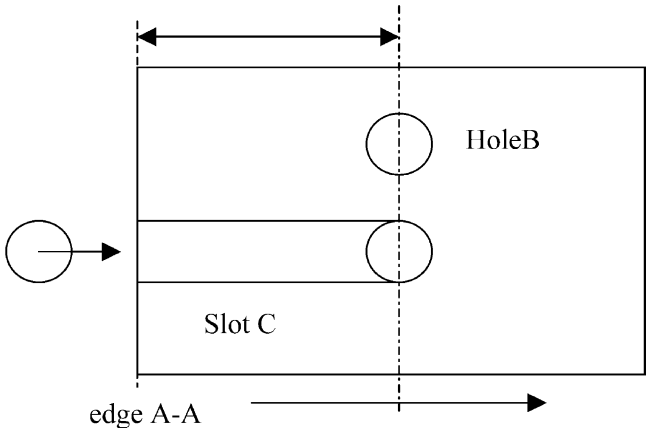

Fig. 11. Slot C and Hole B cutting test along *x* axis in forward direction.

Because the slot cutting force was proportional to tool tip feedrate and tool axial depth of cut, to determine the cutting force induced error, a set of 12 cutting tests were investigated. Table 1 listed all the cutting conditions. The investigation of cutting force induced error in *x* forward and backward directions and *y* forward and backward directions were carried out. All the tests were conducted by a high speed steel end mill cutter with four flutes, 30° helix angle, 11° rake angle, 10 mm diameter, and 30 mm tool overhang. The workpiece was steel SS400. A cutting force sensor was used to measure force in the slot cutting direction. Machining error due to cutting force was measured by a camera.

Fig. 12 show graphs of cutting force average. Fig. 13 show graphs of machining error compared to cutting force.

5.2.2. Cutting force induced error model

Similar to the geometric error model, function approximation by back-propagation neural network was used to approximate cutting forced induced error model. The cutting force was proportional to tool tip

Table 1
Cutting conditions

Test no.	Spindle speed (rpm)	Depth of cut (mm)	Feed rate (mm/min)
Test 1	835	1	50
Test 2	835	1	100
Test 3	835	1	150
Test 4	835	1	200
Test 5	835	2	50
Test 6	835	2	100
Test 7	835	2	150
Test 8	835	2	200
Test 9	835	3	50
Test 10	835	3	100
Test 11	835	3	150
Test 12	835	3	200

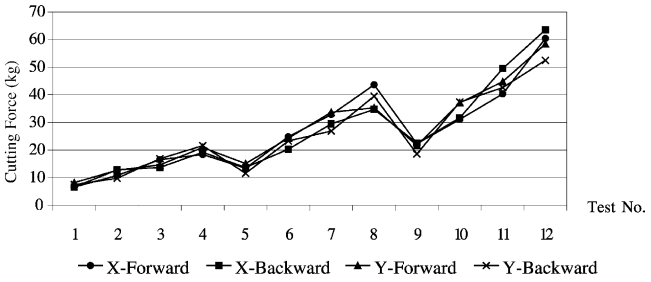

Fig. 12. Cutting force along x and y axis in forward and backward directions.

feedrate and tool axial depth of cut and the machining error due to cutting force was proportional to cutting force. Thus, the machining error due to cutting force was also proportional to cutting force tool tip feedrate and tool axial depth of cut. The back-propagation neural network structure of cutting force induced error model was shown in Fig. 14. Tool tip feedrate and tool axial depth of cut were the input of the network, and machining error due to cutting force were the output of the network.

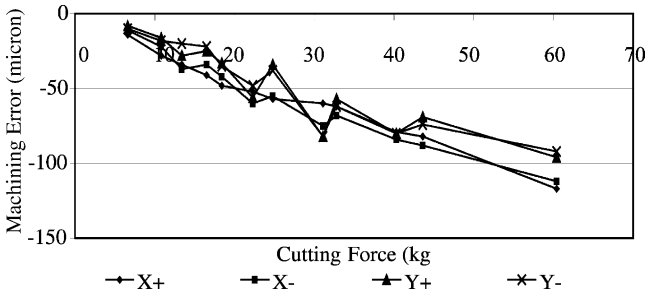

Fig. 13. Cutting force induced error compared to cutting force along x and y axis in forward and backward directions.

Transfer function of the hidden layer was Hyperbolic Tangent Sigmoid and transfer function of the output layer was Linear. The number of nodes in the hidden layer was varied until the approximated mean square error was satisfied at twenty nodes for both forward and backward directions. After training the network, the geometric error could be determined using this model.

5.2.3. *Cutting force induced error compensation*

To evaluate the algorithm, the machining error of four straight line slots cutting on x-y plane moving from point A to B to C to D and to E, as illustrated in Fig. 15, was compensated. The compensation algorithm modified CNC G-code command by subtracting the expected error from the nominal position to reduce error. A set of 4 cutting tests were carried out. Table 2 lists the cutting conditions. All the tests were conducted with the same cutter and workpiece material as in the cutting force error model determination.

5.2.4. *Cutting force induced error compensation results*

Fig. 16 shows the results of the compensated and uncompensated cutting force induced error of tests 1–4. The experimental results show that the average of machining error is improved from −237 to –8 μm for test 1, from −264 to –7 μm for test 2, from −347 to −24 μm for test 3, and from −391 to –20 μm for test 4.

5.3. *Error model combination*

Finally, geometric and cutting force induced errors were considered together using function approximation by back-propagation neural network. The back-propagation neural network structure of the combined model is shown in Fig. 17.

The x, y, z positions, tool tip feedrate and tool axial depth of cut were the input of the network. Geometric

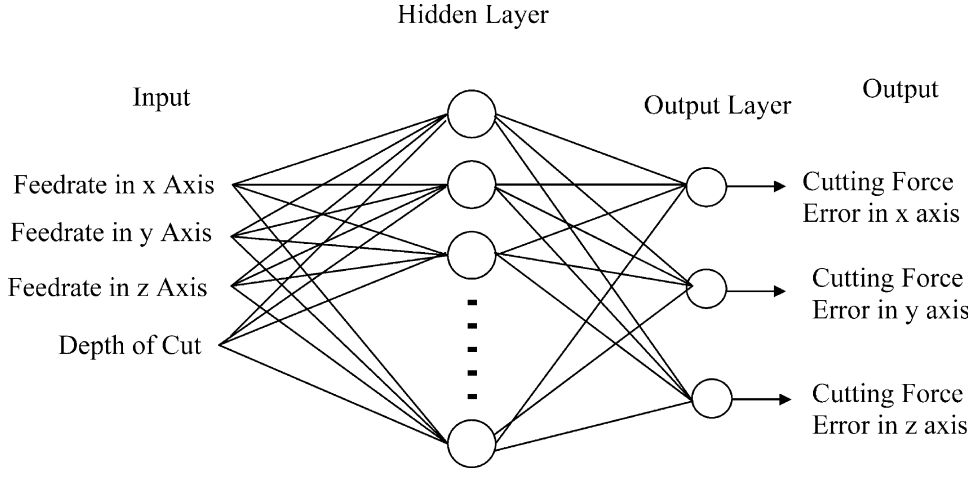

Fig. 14. 4-20-3 Network of cutting force induced error model.

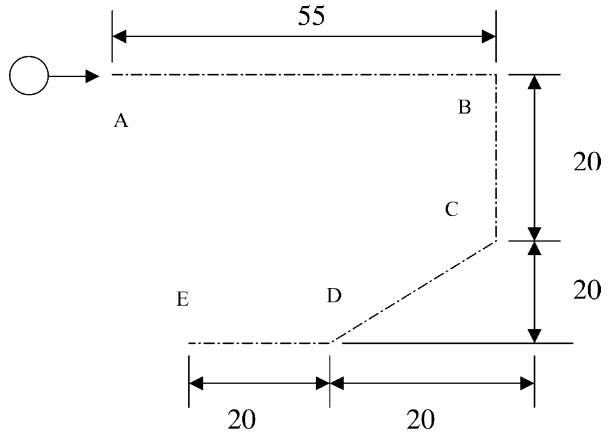

Fig. 15. Cutting path from A to B to C to D and to E.

and cutting force induced errors were the output of the network. Transfer function of the hidden layer was Hyperbolic Tangent Sigmoid and transfer function of the output layer was Linear. The number of nodes in the hidden layer node was varied until the approximated mean square error was satisfied at 110 nodes for both forward and backward directions. After training the network, the resultant error could be determined using this model.

Table 2
Cutting conditions

Test No.	Spindle speed (rpm)	Depth of cut (mm)	Feedrate (mm/min)	Cutting force (kg)
Test 1	835	1	65	8.5
Test 2	835	2	35	10.0
Test 3	835	1.5	70	13.0
Test 4	835	1	130	15.0

6. Conclusions

A new off line error compensation model taking into account geometric and cutting force induced errors in a 3-axis CNC milling machine was proposed in this paper. Geometric and cutting force induced errors in flat end mill of slot cutting were estimated by the proposed model. The geometric error was found highly nonlinear. Estimation of the geometric error at any locations in the working volume was carried out separately by back-propagation neural network. Likewise, estimation of the cutting force induced error was also carried out separately by back-propagation neural network. The combination of geometric and cutting force induced errors was modeled by the combined back-propagation neural network. The unique model was used to compensate both geometric and cutting force induced errors simultaneously by a single model. The experimental results show that by applying the geometric error compensation, the machine accuracy could be improved. From the experiment, the average of improvement of line 1 was approximately −34 and −28 μm in forward and backward directions, respectively. The improvement of line 2 was approximately 44 and 40 μm in forward and backward directions, respectively. The cutting force induced error experimental results show that in slot cutting, the machining error was proportional to cutting force and the average of machining error could be improved from –237 to –8 μm for test 1, from −264 to –7 μm for test 2, from −347 to −24 μm for test 3, and from −391 to –20 μm for test 4. The experimental results show that the machine accuracy was improved significantly.

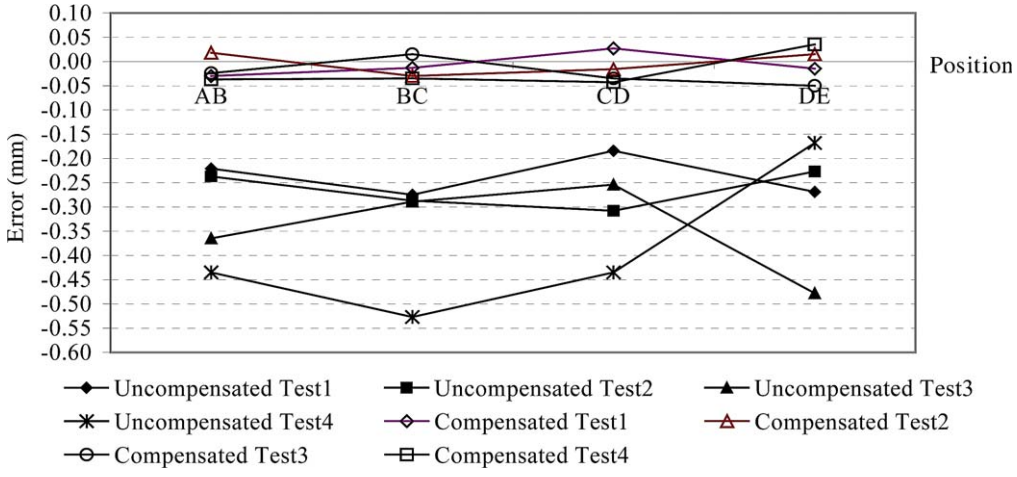

Fig. 16. Error compensation of test 1, test 2, test 3 and test 4.

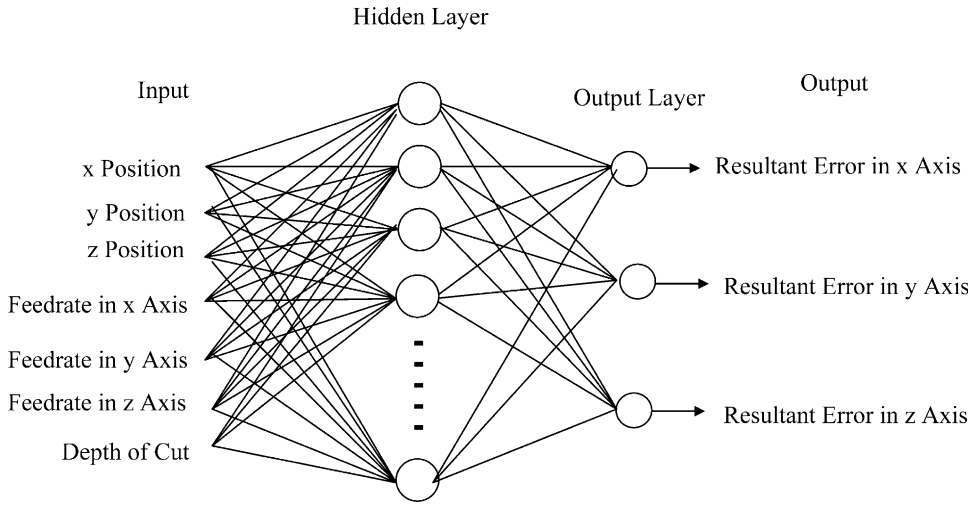

Fig. 17. 7-110-3 Network of error model combination.

Acknowledgements

This research project is financially supported by Mitutoyo Association for Science and Technology.

References

[1] R. Ramesh, M.A. Mannan, A.N. Poo, Error compesation in machine tools—a review Part I: geometric, cutting-force induced and fixture dependent errors, International Journal of machine tools & Manufacture 40 (2000) 1235–1256.

[2] M. Rahman, J. Heikkala, K. Lappalainene, Modeling measurement and error compensation of multi-axis machine tools. Part I: theory, International Journal of Machine Tools & Manufacture 40 (2000) 1535–1546.

[3] K.F. Ehmann, B.T. Wu, M.F. Devries, A generalized geometric error model for multi-axis machines, Annals of CIRP 36 (1) (1987) 253–256.

[4] A.C. Okafor, Y.M. Ertekin, Derivation of machine tool error models and error compensation procedure for three axes vertical machining center using rigid body kinematic, International Journal of Machine Tools and Manufacture 40 (2000) 1199–1213.

[5] C.D. Mize, J.C. Ziegert, Durability evaluation of software error correction on a machine center, International Journal of Machine Tools & Manufacture 40 (2000) 1527–1534.

[6] K.G. Ahn, D.W. Cho, Proposition for a volumetric error consideration backlash in machine tools, The International Journal of Advanced Manufacturing Technology 15 (1999) 554–561.

[7] G. Chen, J. Yuan, J. Ni, A displacement measurement approach for machine geometric assessment, International Journal of Machine Tools & Manufacture 41 (2001) 149–161.

[8] J.S. Chen, T.W. Kou, S.H. Chiou, Geometric error calibration of multi-axis machines using an auto-alignment laser interferometer, Journal of the International Societies for Precision Engineering and Nanotechnology 23 (1999) 243–252.

[9] S.M. Wang, Y.L. Liu, Y. Kang, An efficient error compensation system for CNC multi-axis machines, International Journal of Machine Tools and Manufacture 42 (2002) 1235–1245.

[10] H.F.F. Castro, M. Burdekin, Dynamic calibration of the positioning accuracy of machine tools and coordinate measuring machines using a laser interferometer, International Journal of Machine Tools and Manufacture 43 (2003) 947–954.

[11] W.S. Yun, J.H. Ko, D.W. Cho, K.F. Ehmann, Development of a virtual machining system, part 2 : prediction and analysis of a machined surface error, International Journal of machine tools and Manufacture 42 (2002) 1607–1615.

[12] J.H. Ko, W.S. Yun, D.W. Cho, K.F. Ehmann, Development of a virtual machining system, part 1: approximation of a size effect for cutting force prediction, International Journal of Machine Tools and Manufacture 42 (2002) 1595–1605.

[13] W.S. Yun, D.W. Cho, An improved cutting force model considering the size effect in end milling, ASME International Mechanical Engineering Congress and Exposition, Orlando, FL, 510 November (2000) 223–229.

[14] W.A. Kline, R.E. DeVor, I.A. Shareef, The prediction of surface accuracy in end milling, ASME Journal of Engineering for Industry 104 (1982) 272–278.

[15] G.M. Kim, B.H. Kim, C.N. Chu, Estimation of cutter deflection and form error in ball-end milling process, International Journal of Machine Tools and Manufacture 43 (2003) 917–924.

[16] Y.M. Cheng, J.H. Chin, Machining contour errors as ensembles of cutting, feeding and machine structure effects, International Journal of Machine Tools and Manufacture 43 (2003) 1001–1014.

[17] M.T. Hagan, H.B. Demuth, M. Beale, Neural Network Design, PWS Publishing Company, UK, 1995.